

See discussions, stats, and author profiles for this publication at: <https://www.researchgate.net/publication/323428063>

Evaluating the in vivo glial response to miniaturized parylene cortical probes coated with an ultra-fast degrading polymer to aid insertion

Article in *Journal of Neural Engineering* · June 2018

DOI: 10.1088/1741-2552/aa9fad

CITATIONS

0

READS

156

13 authors, including:



Meng-chen Lo

Massachusetts General Hospital

13 PUBLICATIONS **32** CITATIONS

[SEE PROFILE](#)



Sagar Singh

University of Pennsylvania

14 PUBLICATIONS **28** CITATIONS

[SEE PROFILE](#)



Ijaz Ahmed

Rutgers, The State University of New Jersey

48 PUBLICATIONS **1,139** CITATIONS

[SEE PROFILE](#)



Kevin R Coffey

University of Washington Seattle

19 PUBLICATIONS **50** CITATIONS

[SEE PROFILE](#)

Some of the authors of this publication are also working on these related projects:



Electroporation [View project](#)



Patterned deep brain electrical stimulation to alter inter-region synchronizes within the brain circuits to treat psychiatric disorders. [View project](#)




PAPER

Evaluating the *in vivo* glial response to miniaturized parylene cortical probes coated with an ultra-fast degrading polymer to aid insertion

To cite this article: Meng-chen Lo *et al* 2018 *J. Neural Eng.* **15** 036002

View the [article online](#) for updates and enhancements.

Evaluating the *in vivo* glial response to miniaturized parylene cortical probes coated with an ultra-fast degrading polymer to aid insertion

Meng-chen Lo¹, Shuwu Wang², Sagar Singh¹, Vinod B Damodaran², Ijaz Ahmed¹, Kevin Coffey³, David Barker³, Kshitij Saste², Karanvir Kals², Hilton M Kaplan², Joachim Kohn², David I Shreiber¹ and Jeffrey D Zahn^{1,4}

¹ Department of Biomedical Engineering, Rutgers, The State University of New Jersey, Piscataway, NJ, United States of America

² New Jersey Center for Biomaterials, Rutgers, The State University of New Jersey, Piscataway, NJ, United States of America

³ Department of Psychology, Rutgers, The State University of New Jersey, Piscataway, NJ, United States of America

E-mail: jd Zahn@soe.rutgers.edu

Received 3 February 2017, revised 1 November 2017

Accepted for publication 7 December 2017

Published 27 February 2018



Abstract

Objective. Despite the feasibility of short-term neural recordings using implantable microelectrodes, attaining reliable, chronic recordings remains a challenge. Most neural recording devices suffer from a long-term tissue response, including gliosis, at the device–tissue interface. It was hypothesized that smaller, more flexible intracortical probes would limit gliosis by providing a better mechanical match with surrounding tissue. **Approach.** This paper describes the *in vivo* evaluation of flexible parylene microprobes designed to improve the interface with the adjacent neural tissue to limit gliosis and thereby allow for improved recording longevity. The probes were coated with an ultrafast degrading tyrosine-derived polycarbonate (E5005(2K)) polymer that provides temporary mechanical support for device implantation, yet degrades within 2 h post-implantation. A parametric study of probes of varying dimensions and polymer coating thicknesses were implanted in rat brains. The glial tissue response and neuronal loss were assessed from 72 h to 24 weeks post-implantation via immunohistochemistry. **Main results.** Experimental results suggest that both probe and polymer coating sizes affect the extent of gliosis. When an appropriate sized coating dimension ($100\ \mu\text{m} \times 100\ \mu\text{m}$) and small probe ($30\ \mu\text{m} \times 5\ \mu\text{m}$) was implanted, a minimal post-implantation glial response was observed. No discernible gliosis was detected when compared to tissue where a sham control consisting of a solid degradable polymer shuttle of the same dimensions was inserted. A larger polymer coating ($200\ \mu\text{m} \times 200\ \mu\text{m}$) device induced a more severe glial response at later time points, suggesting that the initial insertion trauma can affect gliosis even when the polymer shuttle degrades rapidly. A larger degree of gliosis was also observed when comparing a larger sized probe ($80\ \mu\text{m} \times 5\ \mu\text{m}$) to a smaller probe ($30\ \mu\text{m} \times 5\ \mu\text{m}$) using the same polymer coating size ($100\ \mu\text{m} \times 100\ \mu\text{m}$). There was no significant neuronal loss around the implantation sites for most device candidates except the group with largest polymer coating and probe sizes. **Significance.** These results suggest that: (1) the degree of mechanical trauma at device implantation and mechanical mismatches

⁴ Author to whom any correspondence should be addressed.

at the probe-tissue interface affect long term gliosis; (2) smaller, more flexible probes may minimize the glial response to provide improved tissue biocompatibility when used for chronic neural signal recording; and (3) some degree of glial scarring did not significantly affect neuronal distribution around the probe.

Keywords: intracortical probe, glial response, flexible probe, biodegradable polymer

(Some figures may appear in colour only in the online journal)

1. Introduction

In recent years, intracortical neural probes have received increased interest as tools to study neuroscience and understand brain functions, and for use in promising therapeutic devices for various biomedical/rehabilitative applications, including neuromodulation, brain-computer interfaces, and neural prosthetics [1–5]. Despite several decades of neural probe development, the ability to achieve consistent long-term neural recordings still remains a major challenge and has prevented the widespread clinical use of intracortical probe technology in humans [6–9]. One of the prominent causes for recording failure is disruption of the electrode-cell interface resulting from the native tissue foreign body response. Implantation of an intracortical probe causes acute, immediate tissue damage including potential disruption of the blood vessels [10, 11], an acute and chronic inflammatory response [12, 13], neural damage and degeneration [14], and ultimately the development of a glial scar [14, 15], which diminishes probe recording quality over time.

Astrocytes and microglia are the two major glial cell types involved in the neural tissue response. Microglia are activated following device implantation and initiate the wound healing response through the secretion of soluble factors, which in turn activate astrocytes, other microglia, immune cells, and cellular pathways through inflammatory cytokines [16, 17]. Activated microglia recruit macrophages which attempt to phagocytize the implanted foreign matter [12, 18, 19]. Although this acute inflammatory response may interrupt probe performance, it usually subsides within a few weeks following device implantation [12, 13]. A longer term chronic tissue response follows, which is characterized by the development of an encapsulation layer around the probe, primarily composed of astrocytes [10, 20, 21]. This glial layer isolates the implant from adjacent neural cells and increases the electrode impedance to neural signal acquisition of local field potentials [22, 23]. Such disruption can cause diminished and/or inconsistent signal quality, which eventually limits the probe's functionality. Most conventional intracortical electrodes (e.g. microwires, Blackrock Microsystems (Utah) arrays, or NeuroNexus (Michigan) arrays) can often sustain recording performance for several months (6–12 months with good signal-to-noise ratio) before the signal quality begins to drop significantly approximately 18–24 months after device implantation [20, 24, 25] until the majority of probes ultimately become incapable of acquiring signals at all.

Various interventions have been investigated to improve the electrode-cell interface and limit the degree of gliosis around

the probes. Some researchers have reported biochemical approaches to limit gliosis by modifying conventional neural probes by incorporating or coating them with substances such as anti-inflammatory drugs (e.g. Dexamethasone (DEX) [26–31], Flavopirido [32]) or neural cell adhesion molecules, such as L1 [33, 34]. Also, by coating the recording electrodes with conductive materials such as carbon nanotubes [35–37] and conductive polymers [31, 38–40], the electrode impedance can also be decreased to allow better electrical integration with neural tissue. These interventions improve probe longevity by reducing the inflammatory response induced by the electrode, enhancing neural cell attachment to the electrode for higher fidelity recording, or increasing the electrode conductivity for improved signal-to-noise ratio.

Another approach to improve the electrode-cell interface is to manipulate device design parameters such as probe size and material. Several studies have shown that subcellular sized probes can significantly reduce the degree of glial scar formation compared to conventional silicon probes and are able to sustain their recording quality for extended periods of time [41–43]. Smaller probes are expected to produce less tissue disruption during device implantation as well as less mechanical mismatch/shearing between the probe and the surrounding tissue. The stiffness of the chosen probe material also contributes to the mechanical mismatch between the neural probe and adjacent tissue layer, where a larger, stiffer probe is expected to have a greater degree of mechanical mismatch, which induces a foreign body response due to the interfacial strain. Furthermore, friction from the device micromotion at the probe-tissue interface has been shown to worsen the inflammatory response and disrupt the cellular microenvironment [44–46]. Several groups have suggested that fabrication of probes from more flexible materials (SU-8 [47, 48], polyimide [49], poly(p-xylylene) (parlylene) [9, 50], shape memory polymers [51, 52], and adaptive polymer nanocomposite materials [53, 54]) that provide a better mechanical match of the device compliance with that of adjacent tissues will minimize tissue responses [55–61].

Fabricating smaller and more flexible (compliant) neural probes represents a promising approach towards attenuating chronic tissue responses. However, implantation of compliant devices can be challenging. Flexible probes are soft and pliable and therefore often buckle during penetration through the meningeal layers. They may also bend and curl easily, leading to device misplacement within the brain. Furthermore, the electronics on the flexible probe can be sensitive to the mechanical forces experienced during insertion and so they need to be protected from distortion and fracture of the electrode traces.

Various techniques have been investigated to aid insertion of flexible probes. One approach is to couple a support such as a needle or silicon shank to the flexible probes as a temporary insertion shuttle, which is often removed after implantation [9, 63–65]. A recent study used a 10 μm wide carbon fiber as an insertion shuttle for a SU-8 based neural probe and showed minimal glial response [63]. Another approach, and our chosen method, is to coat or support the probe with a degradable polymer that is fully resorbed within hours so that no rigid support remains permanently. Several groups have explored coating probes with biodegradable polymers, including silk [65, 66], poly(D,L-lactide-co-glycolide) (PLGA) [67], poly(ethylene glycol) (PEG) [68] and carboxyl-methylcellulose (CMC) [7] to stiffen the devices for cortical implantation. The biodegradable polymers provide temporary support for the probe to withstand insertion forces and then degrade within the tissue, leaving the probe in place for signal acquisition. However, most reports describe a dip-coating method to coat the probes with the supportive polymers. The coating dimensions were less defined and commonly thicker than what is required for insertion ($\sim 200\text{--}500\ \mu\text{m}$) [62, 67]. Dip-coating may also introduce large variabilities in the coating dimensions, as well as increased risk of tissue damage during insertion due to an unnecessarily thick polymer coating. Complications may also be related to extended polymer degradation times and/or non-biocompatible degradation metabolites.

Our group previously reported the biocompatibility of an ultrafast degrading tyrosine-derived polycarbonate E5005(2K) polymer following insertion into rat brain showing minimal astrocyte and microglia activation compared to other degrading polymers such as PLGA and did not show any significant difference in tissue response within randomized implantation sites [69]. When the E5005(2K) polymer was coated onto microwires by dip coating, the tissue response to the microwire showed no significant differences compared to an uncoated control and electrophysiological signal recording capability was demonstrated up to one week after the polymer coating had completely degraded [70]. Building upon this preliminary work, a fabrication process for coating non-functional SU-8 probes with an ultrafast degrading tyrosine-derived polycarbonate (E5005(2K)) was developed [71]. The polymer coating procedure was controlled by molding the polymer within a microchannel structure to ensure consistent dimensions. The coating degraded within 2h post implantation, without disruption of the SU-8 probes. We also reported the development of a finite element model (FEM) to simulate insertion of coated neural probes of varying dimensions and material properties, and identified several possible coating thicknesses which could be used on probe candidates for successful insertion into the brain tissue, and *in vivo* characterization [72]. The computational model predicted that, with the E5005(2K) polymer as a coating material, a minimum coating size of $75\ \mu\text{m} \times 100\ \mu\text{m}$ in cross section would allow 100% of devices to be inserted without buckling or fracture. In this work, we used a more conservative $100\ \mu\text{m} \times 100\ \mu\text{m}$ minimum coating size to ensure successful probe insertion. We also adapted our fabrication process to develop polymer coated microprobes made from parylene. Parylene has emerged as a promising material for fabricating neural probes due to its:

(1) biocompatibility, (2) chemical inertness, and (3) conformal nature (pin-hole free deposition) [73].

The purpose of this study was to perform a parametric study to evaluate the tissue responses to different sized non-functional (lacking electrode traces) probe candidates implanted in a rat model. The effects of different design parameters (probe and polymer coating dimensions) on the acute (72 h) to chronic (up to 24 weeks) glial cell response and neuronal loss around the implantation sites were assessed by the morphological appearance of tissue slices via immunohistochemistry to identify probes sizes and coating dimensions that obviate the glial response to parylene probes. It was hypothesized that a smaller, more flexible intracortical probe would limit gliosis by providing a better mechanical match with surrounding tissue. A secondary investigation was to determine the effect of the coating dimensions on glial cell activation. Results demonstrated that an appropriate sized coating dimension and probe size induced gliosis equivalent to tissue where a blank control consisting of a solid degradable polymer shuttle of the same dimensions was inserted and that the degree of initial insertion trauma can have a direct effect on long term gliosis even when the polymer shuttle degrades rapidly. These results can be used to help guide the design and insertion strategies for flexible probes in order to limit the glial response to functional probes in order to support long term recording fidelity.

2. Materials and methods

2.1. Polymer coated parylene probe fabrication

2.1.1. Polymer preparation. The tyrosine-derived polycarbonate co-polymer was synthesized according to a previously published procedure [74, 75]. This biodegradable polymer has previously been shown to be biologically benign with a tailorable degradation rate. The effect of resorption and degradation kinetics on surrounding brain tissue *in vivo* was previously investigated [70]. These polymers showed minimal astrocyte and microglia activation compared to other degrading polymers such as PLGA. The mechanical and chemical properties of this class of polymers depend on the relative molar percentages of three monomers: desaminotyrosyl-tyrosine alkyl ethyl ester (DTE), desaminotyrosyl-tyrosine (DT), and poly(ethylene glycol) (PEG). The naming convention used for the polymer is EXXYY(MW) as previously described [71], which corresponds to poly(DTE-co-XX%DT-co-YY%-(PEGMW carbonate) where XX is the mole percent of DT, YY is the mole percent of the PEG and the MW is the average molecular weight of the PEG. From the available library of polymers in this class, the specific one used for this study was E5005(2K) ($E = 1.6\ \text{GPa}$, $T_g = 57^\circ\text{C}$, $M_n = 100\text{K}$). The E5005(2K) exhibited optimal properties as an insertion aid, balancing a high Young's modulus, required for device implantation, together with a rapid degradation rate, so that the shuttle degrades into natural (tyrosine) or non-toxic (PEG) metabolites which are cleared from the surrounding tissue within a few hours post-insertion [69–71]. The E5005(2K) polymer solution was prepared as a 9% w/w solution in anhydrous 1, 4-dioxane (Sigma-Aldrich, St. Louis, MO, USA).

2.1.2. Device fabrication. Parylene was chosen as the non-functional probe material. Parylene is a flexible, biocompatible USP Class VI biomaterial that has been widely used for various FDA-approved medical devices [76, 77]. To fabricate the probe, a 5 μm thick parylene layer (Labcoater 2 (PDS 2010), Specialty Coating Systems, Indianapolis, IN, USA) was first deposited onto a glass substrate (figure 1). An aluminum masking layer was then deposited using physical vapor deposition (PVD75, Kurt J. Lesker Company, Jefferson Hills, PA, USA) and patterned using a lift off process to define the probe geometry. The unmasked parylene was isotropically etched using oxygen plasma etching (PX-250, March Instruments, Nordson March Corp., Concord, CA, USA) (600 mTorr, 100 W) for 30 min, which was long enough to etch through a $\sim 7.5 \mu\text{m}$ thick parylene layer and ensure the removal of all of the unmasked parylene layer while defining the probe geometry. The aluminum masking layer was dissolved using aqueous aluminum etchant. The parylene probe was coated with the E5005(2K) degradable polymer according to our previously published procedure [71]. Briefly, a polydimethylsiloxane (PDMS) mold defining the coating dimensions was fabricated by soft lithography and aligned with the parylene probe. The E5005(2K) polymer solution was infused from the molding inlet using the micromolding in capillaries (MIMIC) [78] process, where the polymer solution was introduced into a micro-channel reservoir and filled the cavities through capillary action. The polymer solution was refilled three times to ensure a uniform coating. The polymer coated probe was placed in a vacuum oven under -15 inHg vacuum at $50 \text{ }^\circ\text{C}$ for an hour, and finally in full vacuum (-29.92 inHg) for at least 1 d to ensure complete solvent evaporation. Finally, the PDMS mold was peeled off from the substrate and the probe was lifted off from the substrate using tweezers.

2.2. In vivo characterization using animal models

2.2.1. Polymer-coated probe candidates selection and preparation. The goal of this parametric study was to investigate how the size of the probe and of the polymer coating affects gliosis. Five different designs of varying probe and polymer coating sizes were selected for the study (table 1). Smaller ($100 \mu\text{m} \times 100 \mu\text{m}$) versus larger ($200 \mu\text{m} \times 200 \mu\text{m}$) sized polymer coatings were used to encapsulate the same sized probes to determine whether the initial mechanical trauma induced by the polymer coating during insertion plays a role in long term gliosis (even though the polymer coating rapidly degrades). Different sized probes (no probe, $30 \mu\text{m}$ wide, and $80 \mu\text{m}$ wide) encapsulated within the same polymer coating size ($100 \mu\text{m} \times 100 \mu\text{m}$) were used to determine how cells reacted to the different sized probes after receiving the same insertion trauma. Finally, the probe dimensions of one group (Group 5— $320 \mu\text{m}$ wide) were chosen as a positive control because they matched the width of several probes reported in the literature [9, 62, 79]. A total of ten probes (two from each group) were simultaneously implanted in each animal so that $n = 6$ of each probe type were tested in $n = 3$ animals at each timepoint. The probes were fixed to a custom 3D-printed

surgical holder using epoxy glue to create a single ten-probe assembly. Probes were each spaced $\sim 2 \text{ mm}$ apart from each other, to prevent overlapping tissue response interference. The probe assemblies were treated with UV light (30 min per side) to minimize the risk of infection following implantation. They were then vacuum sealed and stored in a freezer at $-20 \text{ }^\circ\text{C}$ until use. Each device was thawed under vacuum for 15 min prior to implantation to prevent moisture from condensation being absorbed by and damaging the polymer coating.

2.2.2. Surgical procedure. All surgical procedures were performed under a protocol approved by Rutgers' Institutional Animal Care and Use Committee (IACUC). A total of eighteen animals (male Sprague-Dawley rats; Charles River Labs, Wilmington, MA, USA) were used for the study. Each animal was first anesthetized with 5% isoflurane gas, followed by intraperitoneal ketamine (100 mg ml^{-1}) and xylazine (10 mg ml^{-1}). The animal's head was shaved from between the eyes to behind the ears and then fixed in a stereotaxic station. A sagittal incision was made over the midline of the scalp. Bregma and lambda were identified as reference points. Four screws were placed (two on each side, 4 mm from the sagittal suture: the first two 8 mm anterior to bregma and two 4 mm posterior to bregma) to act as anchors for the head stage. Two craniotomies (dimensions shown in figure 2(A)) were drilled 1.5 mm from the midline on each side, anterior to bregma. These implantation locations were selected due to the brain's relative homogeneity and flatness in this region aiming to minimize any variability in the brain tissue between probe sites within each animal as much as possible.

The craniotomies were kept moist with saline. To minimize exposure of the humidity-sensitive polymer-coated probes to the ambient environment, a surrogate surgical assembly with ten non-degradable polymer-coated probes was first fixed to the stereotaxic manipulator. The implantation location was then adjusted to align with the craniotomies, and the precise x - y implantation coordinates were defined (figure 2(B)). Dura was removed prior to device implantation. The surrogate surgical assembly was replaced with the definitive probe assembly, and the probes were inserted manually (at $\sim 2 \text{ mm min}^{-1}$) into the brain. Dental cement (Stoelting Co., Wood Dale, IL, USA) was applied to build a headstage, fixing the probe assembly to the calvarium and anchor screws. The scalp was sutured closed around this headstage. The animal was placed on a water-perfused heating pad until recovery from anesthesia.

2.2.3. Tissue processing and immunohistochemistry. Animals ($n = 3$) were sacrificed at one of six discrete time points (72 h, 10 d, 3 weeks, 7 weeks, 12 weeks and 24 weeks). The animal was first deeply anesthetized with an overdose of pentobarbital. Once the animal reached the surgical plane of anesthesia, it was perfused transcardially with room temperature phosphate buffered saline (PBS) followed by 4% paraformaldehyde ($4 \text{ }^\circ\text{C}$) to fix the tissues. The surgical head stage was removed manually along with the flexible probes. The whole brain was extracted from the skull and preserved in

Parylene probe fabrication and fast degrading polymer coating procedure

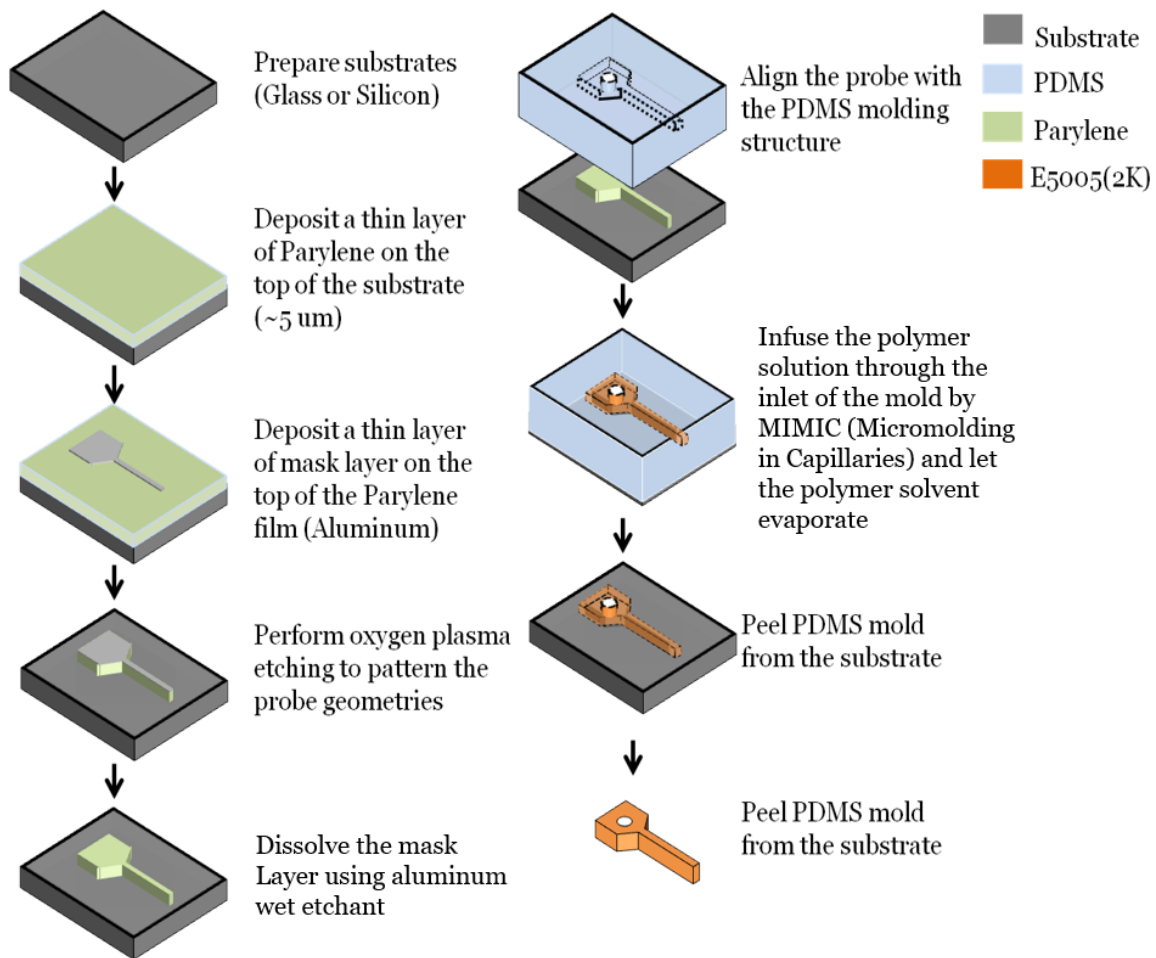


Figure 1. Parylene probe fabrication protocol, polymer coating procedure. First, a thin layer of parylene was deposited. A thin aluminum mask layer that defined the probe geometry was deposited onto the top of the parylene layer with a lift-off method. An oxygen plasma etch was performed to pattern the probe. The mask layer was dissolved with a chemical etchant to complete probe fabrication. The probe was coated with the polymer through MIMIC, and the whole device was dried and released from the substrate [71].

Table 1. Polymer coated parylene probe candidates.

Group	Parylene probe dimensions (width × thickness × length)	Polymer coating dimension (width × thickness × length)	Description
1	30 μm × 5 μm × 3.5 mm	100 μm × 100 μm × 4 mm	Small probe Small coating
2	80 μm × 5 μm × 3.5 mm	100 μm × 100 μm × 4 mm	Large probe Small coating
3	30 μm × 5 μm × 3.5 mm	200 μm × 200 μm × 4 mm	Small probe Large coating
4	None	100 μm × 100 μm × 4 mm	Negative control Small coating only
5	320 μm × 5 μm × 3.5 mm	350 μm × 100 μm × 4 mm	Positive control Similar dimensions to those found in literature [9, 62, 79]

4% paraformaldehyde for 48 h, before transfer into a sucrose-saline cryoprotectant solution until sectioning.

Brain tissue was sectioned in the transverse plane with a cryostat into 30 μm slices. Slices were collected from 1.5 mm, 2 mm, and 2.5 mm deep to the brain’s cranial surface. At each of these levels, immunohistochemistry was performed on

three consecutive slices to label various cell types. For the first slice, the primary antibodies used were specific to: (1) astrocytes: polyclonal chicken anti-gial fibrillary acidic protein (GFAP) (Cat#GFAP, dilution 1:500, Aves Lab, Tigard, OR, USA); and (2) endothelial cells: polyclonal rabbit anti-human Von Willebrand Factor, (Cat#A0082, dilution 1:200,

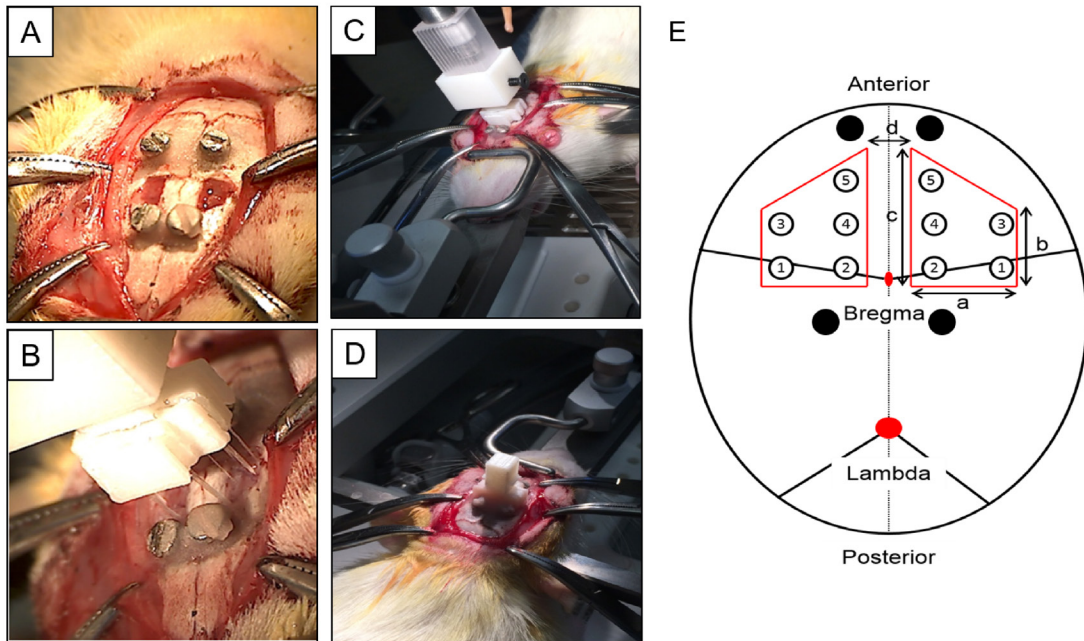


Figure 2. Surgical procedure for the animal study. (A) Two craniotomies were performed. (B), (C) Two probes from each of the five groups were implanted simultaneously via a custom designed surgical holder. (D) Dental cement was used to fix the surgical holder, and the wound was sutured. The animal was placed on a heating pad until recovery from anesthesia. (E) Location and dimension of the two craniotomies and the ten probes (table 1 for number reference) with different dimensions. Black circle display the location of the four skull screws. $A = 4\text{ mm}$; $b = 4\text{ mm}$; $c = 6\text{ mm}$; $d = 3\text{ mm}$.

Dako North America Inc., Carpinteria, CA, USA). The secondary antibodies used were: (1) goat anti-chicken IgY (H + L) (Alexa 647, Cat#A-21449, Life Technologies Inc, Grand Island, NY, USA); and (2) goat anti-rabbit IgY (H + L) (Alexa 488 Cat#A11008, Life Technologies Inc, Grand Island, NY, USA). Endothelial cell identification was used to assist in distinguishing probe implantation sites from blood vessels of similar size. For the second slice, a polyclonal rabbit anti-NeuN (Cat # ab104225, dilution 1:500, Abcam Inc., Cambridge, MA, USA) specific to neurons was used, followed by a goat anti-rabbit IgY (H + L) secondary antibody (Alexa 488 Cat#A11008, dilution 1:500, Life Technologies Inc, Grand Island, NY, USA). For the third slice, the primary antibody was specific to microglia: polyclonal rabbit anti-Iba-1 (Cat#CTK6675, dilution 1:200, Wako Inc., Richmond, VA). The secondary antibody was goat anti-rabbit IgY (H + L) (Alexa 568 Cat#A11011, Life Technologies Inc, Grand Island, NY, USA). Activated microglia were identified by morphology.

2.2.4. Imaging protocol. Immunohistological images were acquired by imaging the entire brain slice using a $4\times$ objective in epifluorescence mode (Olympus IX-81, Waltham, MA, USA) with a CCD camera (Hamamatsu Orca, Hamamatsu Photonics K.K, Hamamatsu City, Shizuoka, Japan). Due to the large overall size of the brain slice, full-brain images were obtained by acquiring multiple images across the brain region and digitally stitching these into a montage image. A grid was applied over the montage to identify individual implantation sites (figure 3). The grid consisted of ten regions of interest (ROIs), each $1\text{ mm} \times 1\text{ mm}$ in size, located over the expected probe

insertion sites according to the surgical assembly dimensions. Each ROI was then reimaged and analyzed at a higher magnification using a $10\times$ objective to quantify cellular responses around each respective implantation site.

2.2.5. Image and data analysis. A Matlab script was developed to perform a rotational intensity sweep profile analysis on individual images of sections from each implantation site (figure 4(A)). The local cell density across the image was correlated to the fluorescence intensity of the labeling antibody at each location. The image was first segmented by thresholding to identify the implantation site. The centroid of the implantation site was identified and set as the starting point for analysis. An end point was defined radially $800\ \mu\text{m}$ from the starting point within an undamaged brain region. The analysis did not exclude the wound sites so that we could also quantify the wound size within each probe group. The end point was selected as a control reference intensity with respect to the implantation sites. Fluorescent label intensity values were obtained along an intensity line trace defined from the starting to the end points. The analysis was repeated in a circular fashion by rotating the line in 1° increments for a full circle sweep. The intensity values were then averaged across the different line traces and normalized to the intensity values of the undamaged area of tissue occurring $600\text{--}800\ \mu\text{m}$ from the implantation center, which was normalized to a fluorescence intensity value of 1.

This approach allowed the assessment of cell behavior around the implantation site for various probe and coating sizes with respect to the distance from the center of the implantation site. The data were further processed to obtain

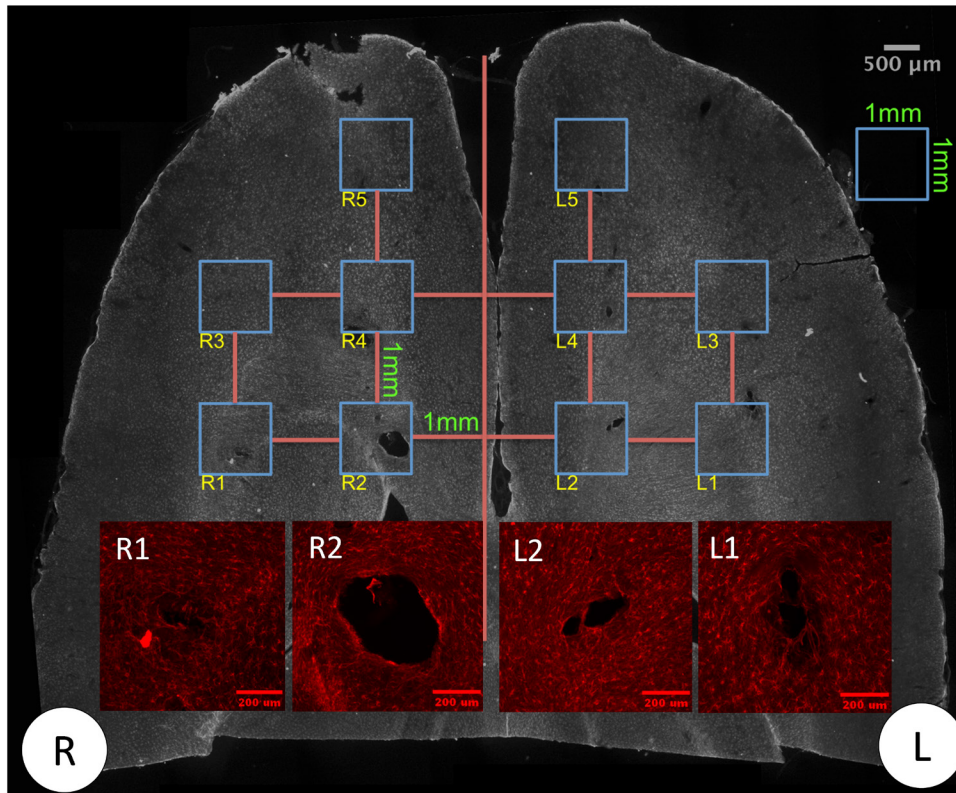


Figure 3. Representative image of (1) a montage of images with a grid for implantation site identification. Scale bar: 500 μm . (2) Inset: magnified images of several implantation sites for downstream image analysis process. Sample ID: 72h control animal sectioned 2 mm deep from the surface of the brain stained with GFAP (astrocytes). R and L indicate right hemisphere and left hemisphere for the animal. Scale bar: 200 μm .

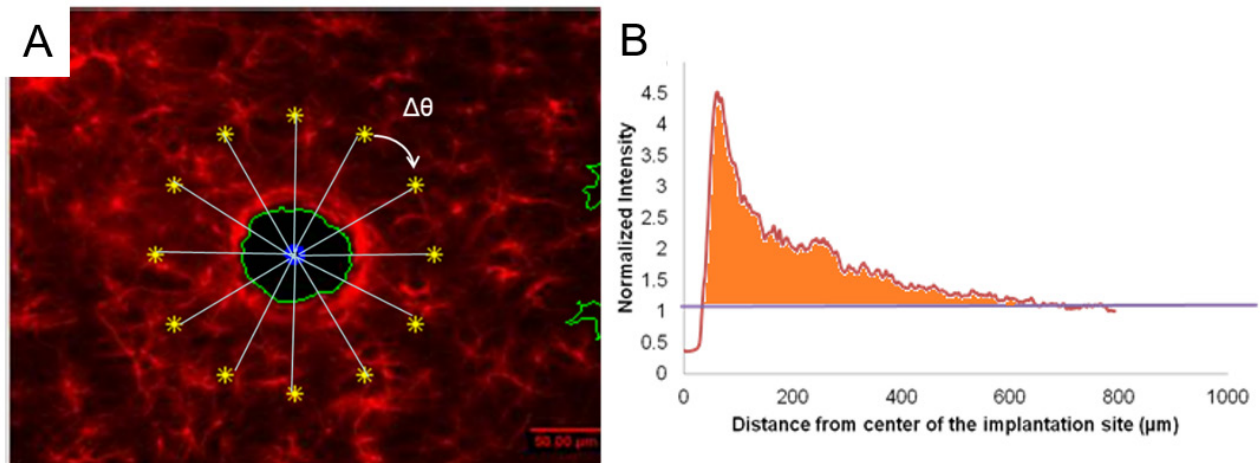


Figure 4. (A) Schematic of the rotational intensity sweep profile analysis. (B) Representative data showing normalized intensity versus distance from the center of the implantation site. The intensity values were normalized by the undamaged area, which was denoted with a value of 1. Area under the curve and above 1 was obtained to indicate the relative image area where the cell density was greater compared to the undamaged area within the region of interest.

a single representative intensity value for comparison among different probe groups, animals, and time points. This representative value was obtained by calculating the total area under the curve when the normalized fluorescence intensity value was above the normalized value of 1, which was indicative of the relative image area where the cell density was comparably greater compared to the undamaged area within the

ROI (i.e. an indication of cellular accumulation around the implantation site) (figure 4(B)). In this manner, the implantation site normalized intensity value was always lower than 1 and excluded from the analysis. One way analysis of variance (ANOVA) was performed to evaluate if there were significant differences ($P < 0.05$) among probe candidates at a specific time point. For time points that were identified as significant

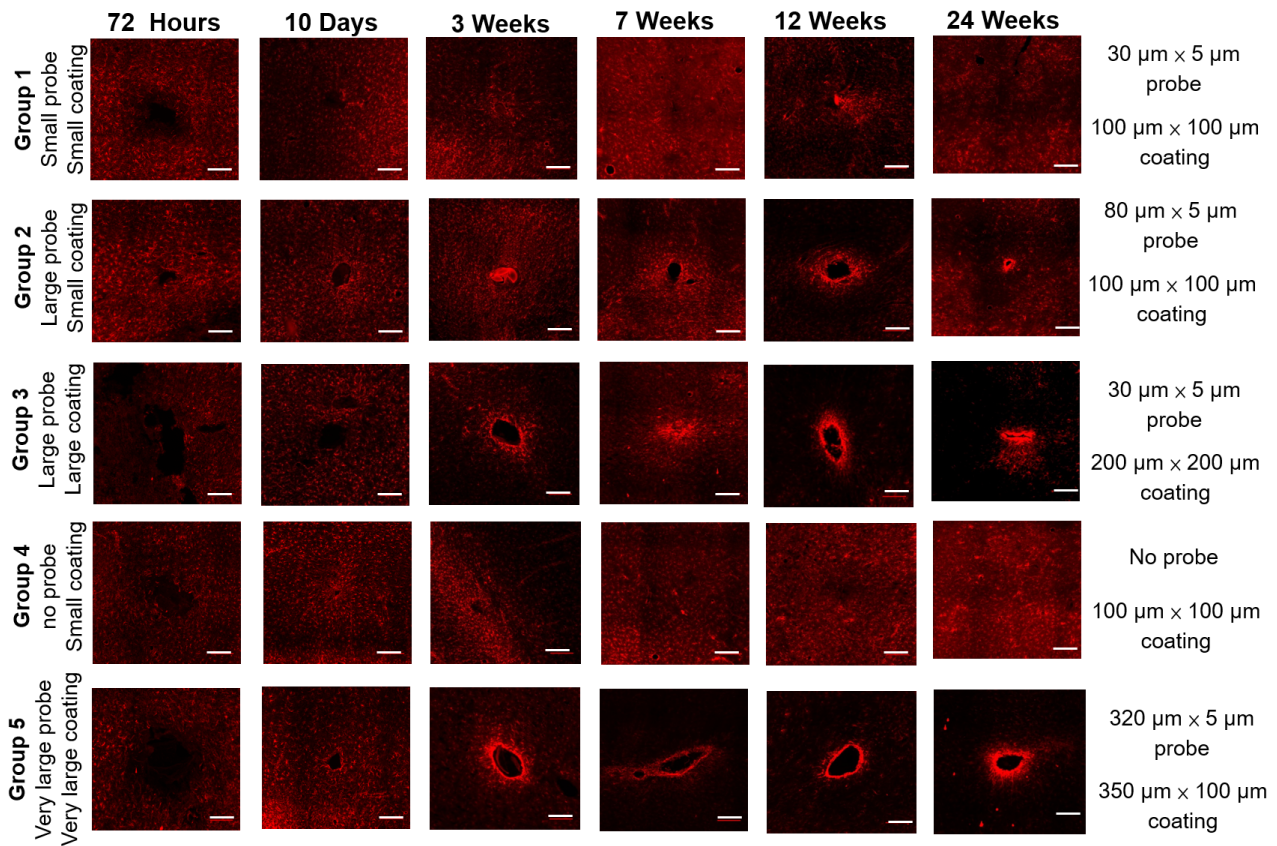


Figure 5. Representative images of GFAP immunostaining for different devices at different time points. Scale bar: 200 μm .

by the omnibus ANOVA, pairwise comparisons with Tukey's post hoc test ($P < 0.05$) were used to identify the devices that were significantly different from each other at that specific time point.

3. Results

3.1. Glial response—astrocyte

Figure 5 displays representative images of GFAP immunofluorescence for each of the five probe candidates at each time point. Figure 6(A) shows the normalized staining intensity and statistical comparisons across different groups at various time points to examine how varying device size and coating dimensions affects glial scar formation. Figures 6(B) and (C) show the average intensity of immunolabeled astrocytes from the center of the implantation sites for all five probe groups at two different time points: 72 h and 24 weeks, respectively. At the 72 h time point, the GFAP intensity was low across all five groups, indicating minimal acute astrocyte activation. Furthermore, GFAP intensity was lower immediately adjacent to the implantation sites for all the groups compared to the undamaged area (figure 6(B)). This might result from tissue necrosis induced by mechanical trauma during insertion or the prevalence of other cell types near the implantation sites. Ten days post device implantation, the GFAP intensity increased, and the insertion wounds had begun to close for all five groups. The groups with the larger polymer coatings (Group 3—200 $\mu\text{m} \times 200 \mu\text{m}$ coating and Group 5—350 $\mu\text{m} \times 100 \mu\text{m}$ coating)

exhibited lower astrocyte density around the implantation site than the groups with the smaller polymer coatings (Groups 1, 2 and 4—100 $\mu\text{m} \times 100 \mu\text{m}$ coating). The groups with the larger polymer coatings created larger wounds upon insertion, which may have prolonged the wound healing time course compared to the groups with the smaller polymer coatings.

At the three-week time point, the astrocyte response started to differentiate among the different groups. A GFAP-positive astrocyte layer formed around the groups with the larger coatings (Group 3—200 $\mu\text{m} \times 200 \mu\text{m}$ coating and Group 5—350 $\mu\text{m} \times 100 \mu\text{m}$ coating). There was a statistically significant GFAP intensity difference between Group 1, the small probe (30 $\mu\text{m} \times 5 \mu\text{m}$ probe) with the small coating (100 $\mu\text{m} \times 100 \mu\text{m}$ coating) and Group 3, the small probe (30 $\mu\text{m} \times 5 \mu\text{m}$ probe) with the large coating (200 $\mu\text{m} \times 200 \mu\text{m}$ coating), suggesting that the larger polymer coating led to a more severe astrocyte response (figure 6(A)). Between groups with the same coating dimensions (100 $\mu\text{m} \times 100 \mu\text{m}$ coating), the larger probe (Group 2—80 $\mu\text{m} \times 5 \mu\text{m}$ probe) induced a higher GFAP intensity compared to the smaller probe (Group 1—30 $\mu\text{m} \times 5 \mu\text{m}$ probe), but the difference was not statistically significant at this time point.

By week seven, the smaller probes in Group 1 showed significantly lower GFAP staining intensity than the larger probes in Group 2 with the same coating size (figure 6(A)). There was no significant difference in GFAP intensity between Group 1 and Group 4, the sham device with no probe. The GFAP intensity remained significantly higher for the coated probes (Group 2) than the coating alone (Group 4). (figure 6(A)).

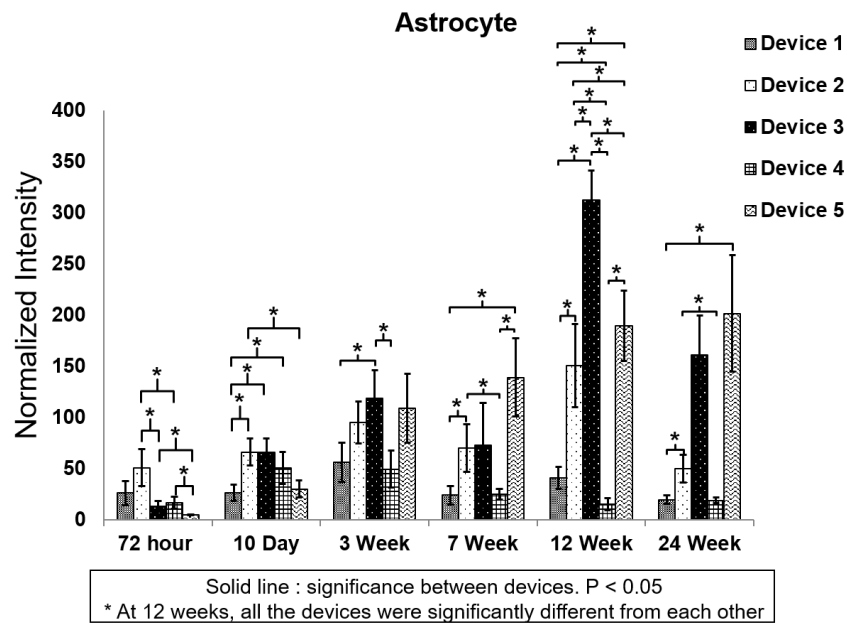


Figure 6. (A) Normalized GFAP intensity at different time points for the five probe groups. *Significance between different groups ($p < 0.05$). **Significance between different groups ($p < 0.01$). ***Significance between different groups ($p < 0.001$). GFAP intensity over the distance from the center of the implantation site for different groups. (B) 72 h post device implantation. (C) 24 weeks post device implantation. The shaded area represents the standard error for each data point.

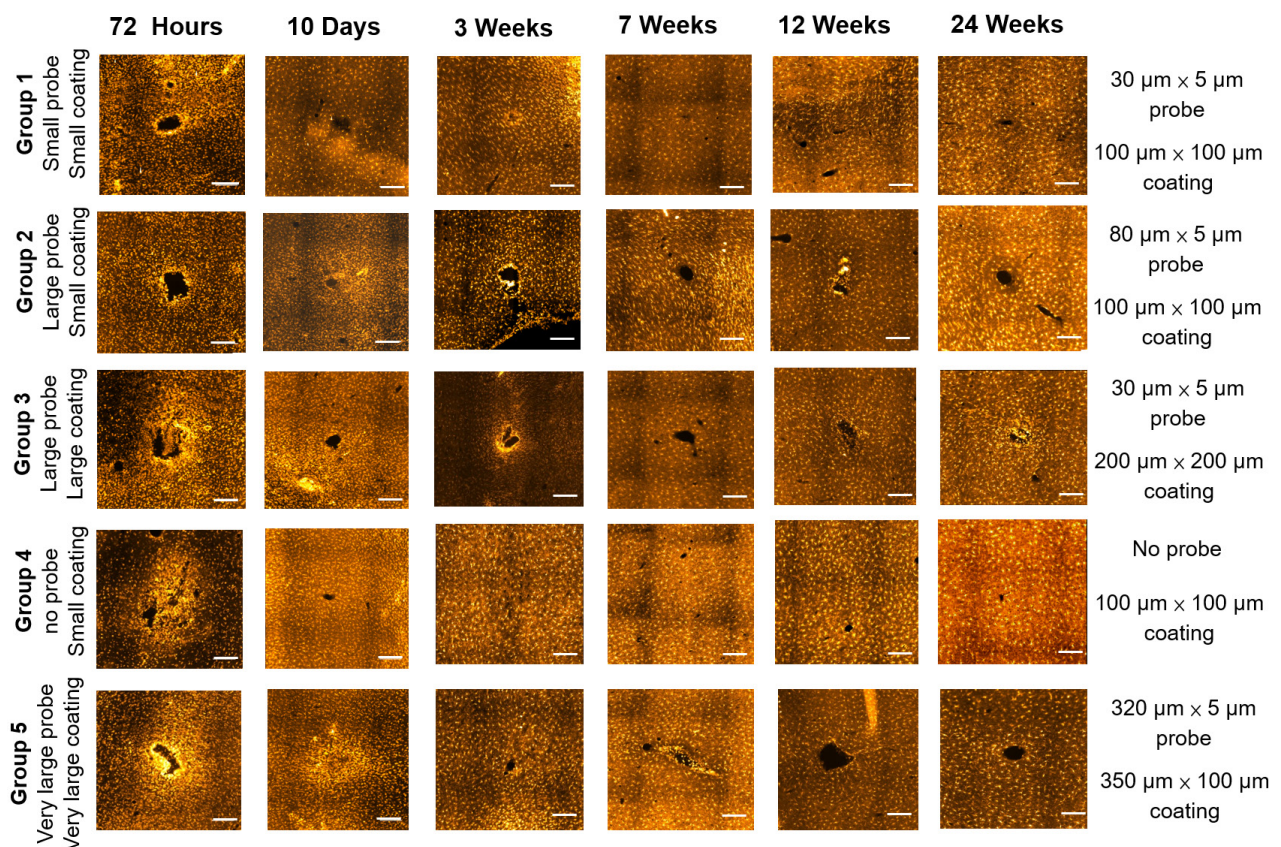


Figure 7. Representative images of Iba-1 immunostaining for different groups at different time points. Scale bar: 200 μm .

These results indicate that the overall probe size plays a role in the glial scar response. As such, to limit astrocyte accumulation, probes would optimally be less than 80 μm wide.

At the 12 week time point, the astrocyte response was significantly different among all groups (figures 5 and 6(A)). The GFAP intensity was positively correlated to the probe sizes for Groups 1, 2, and 4, which have the same coating size. The insertion wounds of most devices in Group 4 (polymer coating only with no probe) were healed and could not be identified (figure 5). The GFAP intensity was also positively correlated to the polymer coating size for Groups 1 and 3, which had the same probe size but different coating dimensions. At this time point, the GFAP intensity was the highest for Group 3 (the 30 $\mu\text{m} \times 5 \mu\text{m}$ probe with the 200 $\mu\text{m} \times 200 \mu\text{m}$ coating) even compared to Group 2 (80 $\mu\text{m} \times 5 \mu\text{m}$ probe with the 100 $\mu\text{m} \times 100 \mu\text{m}$ coating) and Group 5, the largest probe (320 $\mu\text{m} \times 5 \mu\text{m}$ probe) with a large coating (350 $\mu\text{m} \times 100 \mu\text{m}$ coating) indicating that the coated device geometry aspect ratio and/or cross sectional area affected gliosis. The cross-sectional geometry for Group 5 was wider but thinner than for Group 3 and therefore may foster wound closure across the smaller dimension. The increased coating cross-sectional area in Group 3 (200 $\mu\text{m} \times 200 \mu\text{m}$ coating) may lead to more severe acute tissue damage during insertion, which ultimately translates to a more severe chronic astrocyte activation response. These results suggest that overall polymer coating size (and/or cross sectional area) may exhibit a more significant effect on astrocyte response than the overall probe size, despite the polymer coating dissolving at a much earlier time point.

At the 24 week time point (figure 6(C)), the astrocyte response stabilized and subsided compared to week 12. At this time point, the GFAP intensity for the group with smallest implanted probe (Group 1) was not significantly different than the sham, polymer alone group (Group 4). This indicates that the small, flexible probe attenuated astrocyte activation, and therefore the tissue response was minimized. However, the group with the large, 200 $\mu\text{m} \times 200 \mu\text{m}$ coating induced a more severe tissue response comparable to or even more severe than the positive control Group 5.

3.2. Glial response—microglia

Figure 7 displays representative Iba-1 stained images for the five groups at different time points while figure 8 shows the normalized intensity and average intensity traces of immunolabeled microglia from the center of the implantation sites for all five probe groups at 72 h and 24 weeks, respectively. Iba-1 immunolabels both resting and reactive microglia, and morphology was used to identify activated microglia. Quiescent microglia have a highly branched morphology. Upon activation, they begin to proliferate and exhibit an amoeboid morphology [17, 80]. For all of the groups, reactive microglia were observed at the 72 h time point, and a compact layer of microglia was observed around the implantation sites.

The microglial response stabilized 10 d post device implantation. Reactive microglia with an amoeboid morphology were still observed closely packed around the implantation

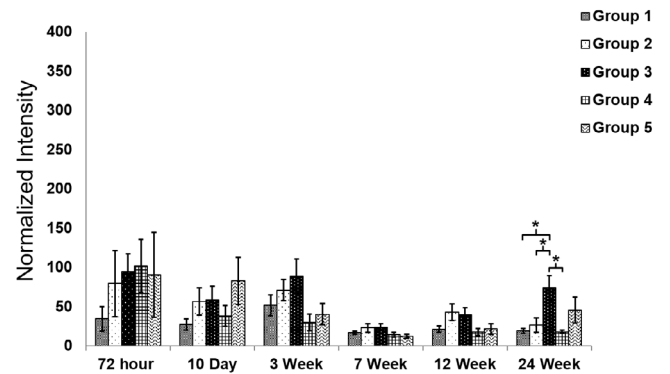


Figure 8. (A) Normalized intensity of Iba-1 staining at different time points for the five probe groups. **Significance between different groups ($p < 0.01$), Iba-1 intensity over the distance from the center of the implantation site for different groups. (B) 72 h post device implantation. (C) 24 weeks post device implantation. The shaded area represents the standard error for each data point.

sites, but the overall intensity decreased compared with the intensity after 72 h (figures 7 and 8(A)). At the three-week time point, the Iba-1 intensity increased for all groups except the pure polymer sham negative control (Group 4). Thus, the acute microglia response induced by insertion trauma was resolved by this three-week time point and had transitioned to a chronic microglial neuro-inflammation response observed in the groups with an encapsulated probe. The time course of microglia activation observed in this study aligns with results reported from several other studies [10, 15, 18].

At the seven and 12 week time points, the chronic response of microglia had decreased and stabilized in all five groups. At the 24 week time point, the microglial response for the groups with the 200 $\mu\text{m} \times 200 \mu\text{m}$ coating (Group 3) and the 320 $\mu\text{m} \times 5 \mu\text{m}$ probe (Group 5) were more severe when compared to the rest of the groups. These results aligned with the astrocyte response observed for the larger probe or coating sizes. Even though the glial scar response consists mainly of astrocytes, microglia have also been observed to reside within the region of gliosis.

3.3. Neuronal response

Figure 9 displays the intensity of immunolabeled neurons over the distance from the center of the implantation sites for all five different groups at two different time points: 72 h and 24 weeks. At the 72 h time point, the 320 $\mu\text{m} \times 5 \mu\text{m}$ probe (Group 5) suffered approximately 20% neuron loss up to 400 μm from the center of the implantation site. This might result from the larger wound size as well as the more severe acute glial cell activation, leaving less space for neurons close to the implantation site. The pure polymer sham negative control (Group 4) exhibited both a smaller wound size and the lowest degree of neuronal loss. Regardless, there was no statistically significant difference in terms of the percentage of neuronal loss among all five groups. At the 24 week time point, the wound size became smaller for each of the probe groups and neurons were found to be located within 50–100 μm of the center of the implantation site. The wound size for the smaller 100 $\mu\text{m} \times 100 \mu\text{m}$ coating groups (Groups 1 and 2)

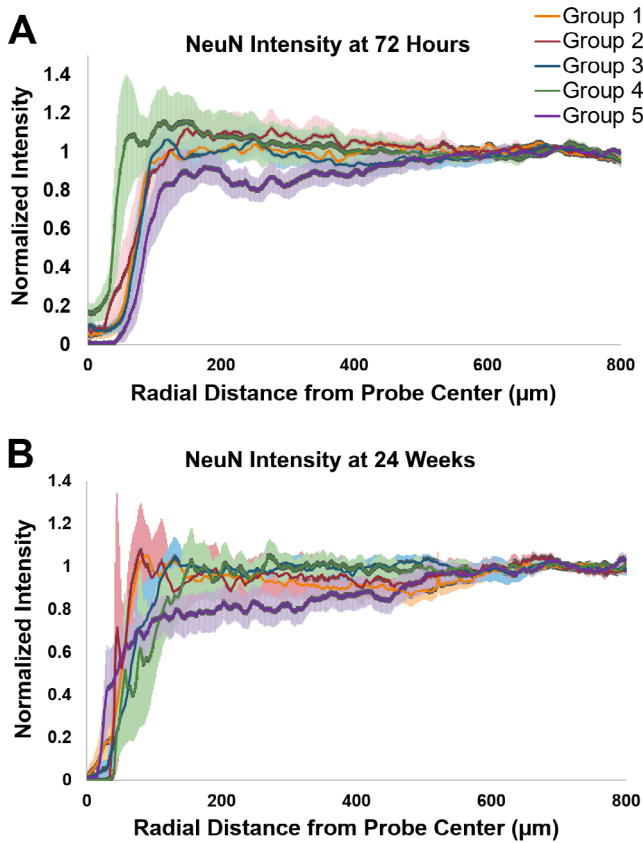


Figure 9. NeuN intensity over the distance from the center of the implantation site for different groups. (A) 72h post device implantation. (B) 24 weeks post device implantation. The shaded area represents the standard error for each data point.

were smaller compared to the larger $200\ \mu\text{m} \times 200\ \mu\text{m}$ and $350\ \mu\text{m} \times 100\ \mu\text{m}$ coating groups (Groups 3 and 5, respectively). The largest $320\ \mu\text{m} \times 5\ \mu\text{m}$ probe (Group 5) resulted in about 10–20% neuron loss up to $500\ \mu\text{m}$ from the center of the implantation site. The rest of the probe groups did not exhibit significant neuronal loss (<10%) around the implantation sites.

4. Discussion

Five device candidates of varying probe and polymer coating sizes were evaluated at six different time points ranging from acute (72h) to chronic (24 weeks), to determine the effects on the development of the glial scar. The biocompatibility of the polymer used for this work was previously studied [70, 74, 81, 82]. In this study, the size of the polymer coating was shown to affect the glial scar, but there was no statistically significant difference in neuronal loss observed around the implantation sites for any of the probe groups.

We previously characterized the polymer coating procedure and degradation profile and demonstrated that the coating degraded within 2h post implantation in an *in vitro* model [71]. Therefore, it was expected that the polymer coating would only affect the short term glial response, and that the probe size would play the primary role in chronic response. When a coating size of $100\ \mu\text{m} \times 100\ \mu\text{m}$ was

used, the larger probes ($80\ \mu\text{m}$ wide \times $5\ \mu\text{m}$ thick) induced a significantly more severe glial response than smaller probes ($30\ \mu\text{m}$ wide \times $5\ \mu\text{m}$ thick) at 7, 12, and 24 week time points. These data support the hypothesis that a smaller and more flexible probe limits gliosis. The larger sized probe is calculated to have ~ 2.67 times the bending stiffness of the smaller probe, which may produce an appreciable increase in interfacial strain due to device micromotion. These results are consistent with many other reports in the literature [44, 45, 83, 84]. Furthermore, the degree of astrocyte activation induced by the small probe was of comparable intensity to that from the smaller pure polymer shank across all time points. Based on these data, we identified the $30\ \mu\text{m}$ wide \times $5\ \mu\text{m}$ thick parylene probe with a $100\ \mu\text{m}$ wide \times $100\ \mu\text{m}$ thick coating as a threshold design to limit the glial scarring, which may improve a device's signal recording consistency.

However, probes of this size and smaller can severely limit the recording potential of the probe. Most conventional neural probes have recording impedances of around $1\ \text{M}\Omega$ at a $1\ \text{kHz}$ recording frequency [85–87]. Previous studies have shown that to achieve this impedance, a recording electrode area of $400\text{--}600\ \mu\text{m}^2$ is typically required. The width of the recording window is usually about $\sim 20\ \mu\text{m}$ diameter. Therefore, a $30\ \mu\text{m}$ wide probe would be the minimum size to support such a recording site. These smaller probes would also limit the number of recording electrodes that can be incorporated within the device. Fewer electrodes allow for less signal acquisition. Thus, probe design requires a balance of signal recording consistency and efficiency, and probes between the 30 and $80\ \mu\text{m}$ widths may need to be investigated to optimally achieve this balance. Coating electrodes with conductive polymers such as poly(3,4-ethylenedioxythiophene) (PEDOT) and poly(pyrrole) (PPy) can also help improve the electrode-cell interface and lower electrical impedance due to their high charge injection capacity, compliant mechanical properties compared to brain tissue, and biocompatibility which may allow smaller electrodes to be used [88].

It was also noted that, for the same sized probe ($30\ \mu\text{m} \times 5\ \mu\text{m}$), the larger polymer coating ($200\ \mu\text{m} \times 200\ \mu\text{m}$) induced a more severe chronic astrocyte response than the smaller polymer coating ($100\ \mu\text{m} \times 100\ \mu\text{m}$). This was a somewhat unexpected result since the coating dimensions are still smaller than other coating strategies such as dip coating, or other insertion strategies such as using a needle or other retractable solid support. It was expected that the coating would resorb within a few hours, and that the influence of the coating dimensions would diminish following wound closure. However, it appears that the more severe mechanical trauma produced by the larger coating led to a sustained increase in the associated acute glial reactivity. These results from the chronic time points indicate that even though the polymer coating is only a few hundred microns in size and degrades within hours, it can also affect the long-term astrocyte response. It appears that if the initial mechanical trauma is too severe, the size and shape of the insertion shuttle can have an impact on the wound healing and glial response, perhaps through disruption of blood vessels and the blood-brain barrier. The increased damage to the microvasculature may sensitize the tissue towards a foreign body insult.

Additionally, a larger wound may not be able to heal and close as effectively as a smaller wound and therefore leads to a more severe long term glial response. A similar phenomenon was reported by Kozai *et al* in which a biodegradable carboxymethyl cellulose (CMC) was used as the insertion shuttle [7]. The wound sites for the majority of the larger CMC shuttles ($300\ \mu\text{m} \times 125\ \mu\text{m}$) never closed and induced a severe astrocyte response, which aligns with our findings and demonstrates the importance of minimizing primary trauma.

We also observed that the microglia response diminished around seven weeks, and that there were no significant differences in microglia activation among the various groups. Microglia are expected to be the main glial cell type residing around implantation sites during the acute tissue response phase. The mechanical insertion trauma activates microglia to phagocytose foreign matter and release inflammatory factors to aid in injury recovery [89–91]. We hypothesize that once the polymer coating was resorbed, the microglia that had initially been activated reverted to a more quiescent phenotype (by week seven). Interestingly, a secondary microglia response was observed at the 24 week time point with Groups 3 and 5, which had larger coatings as well as a parylene probe. The astrocyte cell population is the main component of the long term glial scar layer. However, several studies have also shown that the continued presence of a probe could also induce microglia activation at longer time points [15, 14, 92]. Activated microglia that remain around the implantation site would attempt to phagocytose the foreign material completely.

The initial insertion trauma may also explain the variability in the observed glial cell responses within animals in the same group. Although we implanted the probes in the same anatomical regions, the local brain microvasculature structure will vary from animal to animal. If a probe happens to shear a larger blood vessel during insertion, it may lead to a more severe tissue reaction even for a smaller probe or implant size. Larger sized coatings are, of course, expected to disrupt more blood vessels during insertion which could induce a more severe tissue response.

We also evaluated the neuronal loss around the implantation sites for all five groups at the short term (72 h) and long term (24 week) time points. Only one group (Group 5, $320\ \mu\text{m} \times 5\ \mu\text{m}$ probe with the $350\ \mu\text{m} \times 100\ \mu\text{m}$ coating) demonstrated appreciable neuronal loss (~20%) at both time points. These results are noteworthy as neuronal health is believed to be one of the most essential factors for consistent long term signal acquisition. Although there is evidence that the glial scar can play a beneficial role in encouraging axon regeneration following spinal cord injury [93], there is a general consensus in the literature that, for applications with neural recordings, the glial scar could disturb the cellular environment and adversely affect neuronal health or isolate the probe from adjacent neurons through the glial sheath layer [22, 23]. The minimal neuronal loss in this work suggests that functional probes of similar materials and dimensions may still be able to acquire neuronal signals up to 24 weeks post device implantation. The current study only evaluated the glial and neuronal response of non-functional probes with the focus on the material and

the sizes of the polymer coating and probes. Future work will evaluate the recording capability of functional probes to further investigate the correlation between glial scar formation and electrode performance.

There are some limitations in the study that may affect the results and thus the conclusions. The overall purpose of this work was to parametrically study probe and coating size to identify combinations that limit the glial response as a design tool for further development of functional probes. In this study, all probes were spaced a minimum of 2 mm apart to prevent any contiguous or overlapping tissue responses from adjacent probes. This can be seen in figures 6(B), (C), 8(B), (C) and 9, where the normalized staining intensity is always approximately 1 from $800\ \mu\text{m}$ from the center of the implantation site outward. The probe groups were always implanted at the same location to aid in identifying the implantation sites for each group. This lack of randomization may affect the glial response due to spatial differences in tissue architecture. However, in our previously study by Lewitus *et al*, when the sites were randomized, no significant differences in tissue response were observed [69]. Further, as seen in figure 2(B), Group 2 ($80\ \mu\text{m} \times 5\ \mu\text{m}$ probe, $100\ \mu\text{m} \times 100\ \mu\text{m}$ coating) and Group 3 ($30\ \mu\text{m} \times 5\ \mu\text{m}$ probe, $200\ \mu\text{m} \times 200\ \mu\text{m}$ coating), which displayed the greatest differences in gliosis were always placed adjacent to Group 1 ($30\ \mu\text{m} \times 5\ \mu\text{m}$ probe, $100\ \mu\text{m} \times 100\ \mu\text{m}$ coating) either medially or anteriorly. Thus, the tissue architecture was not expected to vary dramatically between adjacent probes to account for the differences in glial responses observed. Finally, the location of the 4 mm wide coronal strip of brain chosen for implantation was selected due to the relative homogeneity and flatness of the cortex in this region (just anterior to bregma). In future studies, we can decrease the number of the probes implanted in each rat and randomize the implantation sites to adjust for the biological difference within the brain.

Another complication arises from the limited number of probes implanted in each animal due to the sparse probe spacing limiting the number of probes, which could be implanted at a time to ten. Since each probe group was implanted in duplicate in each animal, we chose five experimental probe/coating groups to explore how the probe and coating dimensions affect gliosis including a pure polymer sham control and a large probe group with dimensions comparable to other published reports. Thus, there is no internal control for the $200\ \mu\text{m} \times 200\ \mu\text{m}$ coating size and its influence on gliosis. However, a preliminary experiment conducted showed that the glial isolation layer around a pure $200\ \mu\text{m} \times 200\ \mu\text{m}$ E5005(2K) fast-degrading polymer was minimal four weeks post device implantation (data not shown), and the previous work by Lewitus *et al* [69], a $180\ \mu\text{m}$ cast filament was inserted into rat brain after four weeks showed a glial response comparable to a control craniotomy site (prepped but no implantation conducted). It has been suggested that the polymer degradation products may also influence the glial response. This could be tested by comparing the glial response of an implanted polymer coating of various sizes against a control ‘stab’ wound where the filament is immediately removed following insertion as was conducted by Potter *et al*, using silicon probes [94].

In this work, we demonstrated a method to mechanically augment flexible probes during implantation using an ultra-fast degrading tyrosine-derived polycarbonate. This polymer may be used to coat any neural probe design and does not require any modification of the probe fabrication process or design. Although the polymer coating size was significantly larger than the probe size, our results showed that a pure $100\ \mu\text{m} \times 100\ \mu\text{m}$ coating exhibited minimal glial response and neural loss and therefore could still be an ideal coating size. Moreover, the tyrosine-derived polycarbonate was purely to aid in device insertion. The polymer could be further expanded to incorporate with (1) anti-inflammatory drugs proposed in the literature such as Dexamethasone to help stabilize the wound sites for better wound healing outcomes [26, 31] or neural cell adhesion molecules, such as L1 [33, 34, 95] to help better neuron attachment on the probe for consistent signal acquisition. One advantage of the tyrosine-derived polycarbonate over other polymer candidates such as silk [65, 66] or PEG [68] is its highly tunable degradation properties [82, 96]. Therefore, the release of the drugs or biological molecules can be precisely controlled as desired to maximize the effects over an extended period of time.

5. Conclusions

We have developed small and flexible neural probes, coated with an ultrafast degrading polymer as a temporary aid to insertion into the brain. The effects of different device parameters on glial and neuronal cell response progression were studied over an extended time course using non-functional probes. Our results support the idea that mechanical trauma from device implantation can affect the long-term tissue response. We also showed that the use of the rapidly degrading E5005(2K) polymer as an insertion shuttle could attenuate glial response while remaining amenable to insertion. The tyrosine-derived polycarbonate could also be an ideal carrier as a shuttle to deliver therapeutics or biological molecules to promote wound healing or improve the tissue-electrode interface with highly tunable degradation properties. Finally, we have also observed that the glial response is not well-correlated to neuronal loss around the implantation sites. Future work will investigate the recording performance of the probe and its relationship with both glial scarring and neuronal response.

Acknowledgments

This work was supported by the New Jersey Commission on Spinal Cord Research (NJCSRC) under the grant numbers CSCR12IRG001 and CSCR16IRG007. Any opinions, findings, and conclusions or recommendations expressed in this publication are those of the authors and do not necessarily reflect the views of the NJCSRC.

ORCID iDs

Meng-chen Lo  <https://orcid.org/0000-0003-3913-3233>
 David I Shreiber  <https://orcid.org/0000-0001-8248-419X>
 Jeffrey D Zahn  <https://orcid.org/0000-0001-8712-752X>

References

- [1] Schwartz A B, Cui X T, Weber D J and Moran D W 2006 Brain-controlled interfaces: movement restoration with neural prosthetics *Neuron* **52** 205–20
- [2] Daly J J and Wolpaw J R 2008 Brain-computer interfaces in neurological rehabilitation *Lancet. Neurol.* **7** 1032–43
- [3] Kozai T D Y *et al* 2015 Comprehensive chronic laminar single-unit, multi-unit, and local field potential recording performance with planar single shank electrode arrays *J. Neurosci. Methods* **242** 15–40
- [4] Fernandez E *et al* 2014 Acute human brain responses to intracortical microelectrode arrays: challenges and future prospects *Front. Neuroeng.* **7** 1–6
- [5] Gunasekera B, Saxena T, Bellamkonda R and Karumbaiah L 2015 Intracortical recording interfaces: current challenges to chronic recording function *ACS Chem. Neurosci.* **6** 68–83
- [6] Fekete Z 2015 Recent advances in silicon-based neural microelectrodes and microsystems: a review *Sensors Actuators B* **215** 300–15
- [7] Kozai T D Y *et al* 2014 Chronic tissue response to carboxymethyl cellulose based dissolvable insertion needle for ultra-small neural probes *Biomaterials* **35** 9255–68
- [8] Polikov V S, Tresco P A and Reichert W M 2005 Response of brain tissue to chronically implanted neural electrodes *J. Neurosci. Methods* **148** 1–18
- [9] Kim B J *et al* 2013 3D Parylene sheath neural probe for chronic recordings *J. Neural Eng.* **10** 045002
- [10] Turner J N *et al* 1999 Cerebral astrocyte response to micromachined silicon implants *Exp. Neurol.* **156** 33–49
- [11] Saxena T *et al* 2013 The impact of chronic blood-brain barrier breach on intracortical electrode function *Biomaterials* **34** 4703–13
- [12] Fujita T, Yoshimine T, Maruno M and Hayakawa T 1998 Cellular dynamics of macrophages and microglial cells in reaction to stab wounds in rat cerebral cortex *Acta Neurochir.* **140** 275–9
- [13] Leskovaar A, Moriarty L, Turek J, Schoenlein I and Borgens R 2000 The macrophage in acute neural injury: changes in cell numbers over time and levels of cytokine production in mammalian central and peripheral nervous systems *J. Exp. Biol.* **203** 1783–95
- [14] Biran R, Martin D C and Tresco P A 2005 Neuronal cell loss accompanies the brain tissue response to chronically implanted silicon microelectrode arrays *Exp. Neurol.* **195** 115–26
- [15] Szarowski D H *et al* 2003 Brain responses to micro-machined silicon devices *Brain Res.* **983** 23–35
- [16] Kozai T D Y, Jaquins-Gerstl A S, Vazquez A L, Michael A C and Cui X T 2016 Dexamethasone retrodialysis attenuates microglial response to implanted probes *in vivo* *Biomaterials* **87** 157–69
- [17] Nimmerjahn A, Kirchhoff F and Helmchen F 2005 Resting microglial cells are highly dynamic surveillants of brain parenchyma *in vivo* *Science* **308** 1314–8
- [18] Giordana M T *et al* 1994 Reactive cell proliferation and microglia following injury to the rat brain *Neuropathol. Appl. Neurobiol.* **20** 163–74
- [19] Vetter R J, Williams J C, Hetke J F, Nunamaker E A and Kipke D R 2004 Chronic neural recording using silicon-substrate microelectrode arrays implanted in cerebral cortex *IEEE Trans. Biomed. Eng.* **51** 896–904
- [20] Rousche P J and Normann R A 1998 Chronic recording capability of the Utah Intracortical Electrode Array in cat sensory cortex *J. Neurosci. Methods* **82** 1–15
- [21] Edell D J, Toi V V, McNeil V M and Clark L D 1992 Factors influencing the biocompatibility of insertable silicon microshafts in cerebral cortex *Biomed. Eng. IEEE Trans.* **39** 635–43

- [22] Mercanzini A, Colin P, Bensadoun J C, Bertsch A and Renaud P 2009 *In vivo* electrical impedance spectroscopy of tissue reaction to microelectrode arrays *IEEE Trans. Biomed. Eng.* **56** 1909–18
- [23] Williams J C, Hippensteel J A, Dilgen J, Shain W and Kipke D R 2007 Complex impedance spectroscopy for monitoring tissue responses to inserted neural implants *J. Neural Eng.* **4** 410–23
- [24] Williams J C, Rennaker R L and Kipke D R 1999 Long-term neural recording characteristics of wire microelectrode arrays implanted in cerebral cortex *Brain Res. Protoc.* **4** 303–13
- [25] Nicolelis M A L *et al* 2003 Chronic, multisite, multielectrode recordings in macaque monkeys *Proc. Natl Acad. Sci. USA* **100** 11041–6
- [26] Zhong Y and Bellamkonda R V 2007 Dexamethasone-coated neural probes elicit attenuated inflammatory response and neuronal loss compared to uncoated neural probes *Brain Res.* **1148** 15–27
- [27] Abidian M R, Kim D-H and Martin D C 2006 Conducting-polymer nanotubes for controlled drug release *Adv. Mater.* **18** 405–9
- [28] Spataro L *et al* 2005 Dexamethasone treatment reduces astroglia responses to inserted neuroprosthetic devices in rat neocortex *Exp. Neurol.* **194** 289–300
- [29] Kim D-H and Martin D C 2006 Sustained release of dexamethasone from hydrophilic matrices using PLGA nanoparticles for neural drug delivery *Biomaterials* **27** 3031–7
- [30] Lee C D *et al* 2016 Matrigel coatings for Parylene sheath neural probes *J. Biomed. Mater. Res. B* **104** 357–68
- [31] Boehler C *et al* 2017 Actively controlled release of Dexamethasone from neural microelectrodes in a chronic *in vivo* study *Biomaterials* **129** 176–87
- [32] Purcell E K, Thompson D E, Ludwig K A and Kipke D R 2009 Flavopiridol reduces the impedance of neural prostheses *in vivo* without affecting recording quality *J. Neurosci. Methods* **183** 149–57
- [33] Azemi E, Lagenaur C F and Cui X T 2011 The surface immobilization of the neural adhesion molecule L1 on neural probes and its effect on neuronal density and gliosis at the probe/tissue interface *Biomaterials* **32** 681–92
- [34] Kolarcik C L *et al* 2012 *In vivo* effects of L1 coating on inflammation and neuronal health at the electrode–tissue interface in rat spinal cord and dorsal root ganglion *Acta Biomater.* **8** 3561–75
- [35] Baretke-Keren L and Hanein Y 2013 Carbon nanotube-based multi electrode arrays for neuronal interfacing: progress and prospects *Front. Neural Circuits* **6** 122
- [36] Keefer E W, Botterman B R, Romero M I, Rossi A F and Gross G W 2008 Carbon nanotube coating improves neuronal recordings *Nat. Nanotechnol.* **3** 434–9
- [37] Fang S-P *et al* 2016 A carbon nanofiber (CNF) based 3D microelectrode array for *in vitro* neural proliferation and signal recording 2016 *IEEE 29th Int. Conf. on Micro Electro Mechanical Systems* (IEEE) pp 423–6 (<https://doi.org/10.1109/MEMSYS.2016.7421651>)
- [38] Abidian M R, Corey J M, Kipke D R and Martin D C 2010 Conducting-polymer nanotubes improve electrical properties, mechanical adhesion, neural attachment, and neurite outgrowth of neural electrodes *Small* **6** 421–9
- [39] Vitale F, Summerson S R, Aazhang B, Kemere C and Pasquali M 2015 Neural stimulation and recording with bidirectional, soft carbon nanotube fiber microelectrodes *ACS Nano* **9** 4465–74
- [40] Kozai T *et al* 2015 Chronic *in vivo* evaluation of PEDOT/CNT for stable neural recordings *IEEE Trans. Biomed. Eng.* **63** 111–9
- [41] Kang M *et al* 2014 Subcellular neural probes from single-crystal gold nanowires *ACS Nano* **8** 8182–9
- [42] Seymour J P and Kipke D R 2007 Neural probe design for reduced tissue encapsulation in CNS *Biomaterials* **28** 3594–607
- [43] Kozai T D Y *et al* 2012 Ultrasmall implantable composite microelectrodes with bioactive surfaces for chronic neural interfaces *Nat. Mater.* **11** 1065–73
- [44] Harrison D G *et al* 2006 Endothelial mechanotransduction, nitric oxide and vascular inflammation *J. Intern. Med.* **259** 351–63
- [45] Lund T *et al* 2010 Shear stress regulates inflammatory and thrombogenic gene transcripts in cultured human endothelial progenitor cells *Thromb. Haemost.* **104** 582–91
- [46] Uhlig S 2002 Ventilation-induced lung injury and mechanotransduction: stretching it too far? *Am. J. Physiol. Lung Cell. Mol. Physiol.* **282** L892–6
- [47] Altuna A *et al* 2012 SU-8 based microprobes with integrated planar electrodes for enhanced neural depth recording *Biosens. Bioelectron.* **37** 1–5
- [48] Cho S-H *et al* 2008 Biocompatible SU-8-based microprobes for recording neural spike signals from regenerated peripheral nerve fibers *IEEE Sens. J.* **8** 1830–6
- [49] Fukushima M *et al* 2014 An electrocorticographic electrode array for simultaneous recording from medial, lateral, and intrasulcal surface of the cortex in macaque monkeys *J. Neurosci. Methods* **233** 155–65
- [50] Takeuchi S, Ziegler D, Yoshida Y, Mabuchi K and Suzuki T 2005 Parylene flexible neural probes integrated with microfluidic channels *Lab Chip* **5** 519–23
- [51] Zhao Q, Qi H J and Xie T 2015 Recent progress in shape memory polymer: new behavior, enabling materials, and mechanistic understanding *Prog. Polym. Sci.* (<https://doi.org/10.1016/j.progpolymsci.2015.04.001>)
- [52] Jorfi M *et al* 2015 Mechanically adaptive materials for intracortical implants 2015 *7th Int. IEEE/EMBS Conf. on Neural Engineering* (IEEE) pp 601–2 (<https://doi.org/10.1109/NER.2015.7146694>)
- [53] Hess-Dunning A E *et al* 2014 Microscale characterization of a mechanically adaptive polymer nanocomposite with cotton-derived cellulose nanocrystals for implantable BioMEMS *J. Microelectromech. Syst.* **23** 774–84
- [54] Nguyen J K *et al* 2016 Influence of resveratrol release on the tissue response to mechanically adaptive cortical implants *Acta Biomater.* **29** 81–93
- [55] Stieglitz T, Beutel H, Blau C and Meyer J U 1997 Flexible multichannel microelectrodes with integrated leads for use in neuroprosthetics *Biomed. Technol.* **42** 449–50
- [56] Takeuchi S and Shimoyama I 2000 Three-dimensional shape memory alloy microelectrode with clipping structure for insect neural recording *J. Microelectromech. Syst.* **9** 24–31
- [57] Hoogerwerf A C and Wise K D 1994 A three-dimensional microelectrode array for chronic neural recording *IEEE Trans. Biomed. Eng.* **41** 1136–46
- [58] Sridharan A, Nguyen J K, Capadona J R and Muthuswamy J 2015 Compliant intracortical implants reduce strains and strain rates in brain tissue *in vivo* *J. Neural Eng.* **12** 036002
- [59] Barz F, Ruther P, Takeuchi S and Paul O 2015 Flexible silicon-polymer neural probe rigidified by dissolvable insertion vehicle for high-resolution neural recording with improved duration 2015 *28th IEEE Int. Conf. on Micro Electro Mechanical Systems* (IEEE) pp 636–9 (<https://doi.org/10.1109/MEMSYS.2015.7051036>)
- [60] Fan B, Rechenberg R, Becker M F and Li W 2015 Fabrication of polycrystalline diamond on a flexible Parylene substrate 2015 *Transducers—2015 18th Int. Conf. on Solid-State Sensors, Actuators and Microsystems (TRANSDUCERS)* pp 892–5 (IEEE) (<https://doi.org/10.1109/TRANSDUCERS.2015.7181067>)
- [61] Schander A *et al* 2015 Design and fabrication of multi-contact flexible silicon probes for intracortical floating implantation

- 2015 *Transducers—2015 18th Int. Conf. on Solid-State Sensors, Actuators and Microsystems (TRANSDUCERS)* (IEEE) pp 1739–42 (<https://doi.org/10.1109/TRANSDUCERS.2015.7181281>)
- [62] Felix S H *et al* 2013 Insertion of flexible neural probes using rigid stiffeners attached with biodissolvable adhesive *J. Vis. Exp.* **e50609**
- [63] Luan L *et al* 2017 Ultraflexible nanoelectronic probes form reliable, glial scar-free neural integration *Sci. Adv.* **3** e1601966
- [64] Köhler P *et al* 2015 Influence of probe flexibility and gelatin embedding on neuronal density and glial responses to brain implants *PLoS One* **10** e0119340
- [65] Hwang S-W *et al* 2014 High-performance biodegradable/transient electronics on biodegradable polymers *Adv. Mater.* **26** 3905–11
- [66] Kundu B *et al* 2014 Silk proteins for biomedical applications: bioengineering perspectives *Prog. Polym. Sci.* **39** 251–67
- [67] Foley C, Nishimura N, Neeves K, Schaffer C and Olbricht W 2009 Flexible microfluidic devices supported by biodegradable insertion scaffolds for convection-enhanced neural drug delivery *Biomed. Microdevices* **11** 915–24
- [68] Chen C-H *et al* 2009 Three-dimensional flexible microprobe for recording the neural signal 2009 *IEEE Int. Conf. on Nano/Molecular Medicine and Engineering* pp 278–81 (<https://doi.org/10.1109/nanomed.2009.5559071>)
- [69] Lewitus D Y, Smith K L, Shain W, Bolikal D and Kohn J 2011 The fate of ultrafast degrading polymeric implants in the brain *Biomaterials* **32** 5543–50
- [70] Lewitus D, Smith K L, Shain W and Kohn J 2011 Ultrafast resorbing polymers for use as carriers for cortical neural probes *Acta Biomater.* **7** 2483–91
- [71] Lo M *et al* 2015 Coating flexible probes with an ultra fast degrading polymer to aid in tissue insertion *Biomed. Microdevices* **17** 34
- [72] Singh S *et al* 2016 Modeling the insertion mechanics of flexible neural probes coated with sacrificial polymers for optimizing probe design *Sensors* **16** 330
- [73] Senkevich J J and Wang P-I 2009 Molecular layer chemistry via parylenes *Chem. Vap. Depos.* **15** 91–4
- [74] Schut J *et al* 2007 Glass transition temperature prediction of polymers through the mass-per-flexible-bond principle *Polymer* **48** 6115–24
- [75] Rojas R, Harris N K, Piotrowska K and Kohn J 2009 Evaluation of automated synthesis for chain and step-growth polymerizations: can robots replace the chemists? *J. Polym. Sci. A* **47** 49–58
- [76] Westedt U *et al* 2006 Paclitaxel releasing films consisting of poly(vinyl alcohol)-graft-poly(lactide-co-glycolide) and their potential as biodegradable stent coatings *J. Control. Release* **111** 235–46
- [77] Rodger D C and Humayun M S 2008 Implantable parylene-based wireless intraocular pressure sensor 2008 *IEEE 21st Int. Conf. on Micro Electro Mechanical Systems* (IEEE) pp 58–61 (<https://doi.org/10.1109/MEMSYS.2008.4443592>)
- [78] Kim E, Xia Y and Whitesides G M 1996 Micromolding in capillaries: applications in materials science *J. Am. Chem. Soc.* **118** 5722–31
- [79] Kim E G R *et al* 2014 A hybrid silicon-parylene neural probe with locally flexible regions *Sensors Actuators B* **195** 416–22
- [80] Tremblay M-È, Lowery R L and Majewska A K 2010 Microglial interactions with synapses are modulated by visual experience *PLoS Biol.* **8** e1000527
- [81] Hooper K A, Macon N D and Kohn J 1998 Comparative histological evaluation of new tyrosine-derived polymers and poly(L-lactic acid) as a function of polymer degradation *J. Biomed. Mater. Res.* **41** 443–54
- [82] Bourke S L and Kohn J 2003 Polymers derived from the amino acid L-tyrosine: polycarbonates, polyarylates and copolymers with poly(ethylene glycol) *Adv. Drug Deliv. Rev.* **55** 447–66
- [83] Waters C M 2004 Reactive oxygen species in mechanotransduction *Am. J. Physiol. Lung Cell. Mol. Physiol.* **287** L484–5
- [84] Subbaroyan J *et al* 2005 A finite-element model of the mechanical effects of implantable microelectrodes in the cerebral cortex *J. Neural Eng.* **2** 103–13
- [85] Cogan S F 2008 Neural stimulation and recording electrodes *Annu. Rev. Biomed. Eng.* **10** 275–309
- [86] Ward M P, Rajdev P, Ellison C and Irazoqui P P 2009 Toward a comparison of microelectrodes for acute and chronic recordings *Brain Res.* **1282** 183–200
- [87] Karp F B, Bernotski N A, Valdes T I, Bohringer K F and Ratner B D 2008 Foreign body response investigated with an implanted biosensor by *in situ* electrical impedance spectroscopy *IEEE Sens. J.* **8** 104–12
- [88] Harris A R *et al* 2013 Conducting polymer coated neural recording electrodes *J. Neural Eng.* **10** 016004
- [89] Banati R B, Gehrman J, Schubert P and Kreutzberg G W 1993 Cytotoxicity of microglia *Glia* **7** 111–8
- [90] Woodroffe M N *et al* 1991 Detection of interleukin-1 and interleukin-6 in adult rat brain, following mechanical injury, by *in vivo* microdialysis: evidence of a role for microglia in cytokine production *J. Neuroimmunol.* **33** 227–36
- [91] Nakajima K *et al* 2001 Neurotrophin secretion from cultured microglia *J. Neurosci. Res.* **65** 322–31
- [92] Gentleman S M *et al* 2004 Long-term intracerebral inflammatory response after traumatic brain injury *Forensic Sci. Int.* **146** 97–104
- [93] Anderson M A *et al* 2016 Astrocyte scar formation aids central nervous system axon regeneration *Nature* **532** 195–200
- [94] Potter K A, Buck A C, Self W K and Capadona J R 2012 Stab injury and device implantation within the brain results in inversely multiphasic neuroinflammatory and neurodegenerative responses *J. Neural Eng.* **9** 046020
- [95] Eles J R *et al* 2017 Neuroadhesive L1 coating attenuates acute microglial attachment to neural electrodes as revealed by live two-photon microscopy *Biomaterials* **113** 279–92
- [96] Magno M H R *et al* 2010 Synthesis, degradation and biocompatibility of tyrosine-derived polycarbonate scaffolds *J. Mater. Chem.* **20** 8885